In operando plasmonic monitoring of electrochemical evolution of lithium metal

Yan Jin[a,b], Lin Zhou[a,b,c,1], Jianyu Yu[a,b], Jie Liang[a,b], Wenshan Cai[d], Huigang Zhang[a,b], Shining Zhu[a,b,c], and Jia Zhu[a,b,1]

[a]National Laboratory of Solid State Microstructures, College of Engineering and Applied Sciences, School of Physics, Nanjing University, 210093 Nanjing, P. R. China; [b]Collaborative Innovation Center of Advanced Microstructures, Nanjing University, 210093 Nanjing, P. R. China; [c]Key Laboratory of Intelligent Optical Sensing and Integration, Nanjing University, 210093 Nanjing, P. R. China; and [d]School of Electrical and Computer Engineering, Georgia Institute of Technology, Atlanta, GA 30332

Edited by Peidong Yang, Lawrence Berkeley National Laboratory, University of California, Berkeley, CA, and approved September 20, 2018 (received for review May 18, 2018)

The recent renaissance of lithium metal batteries as promising energy storage devices calls for in operando monitoring and control of electrochemical evolution of lithium metal morphologies. While the development of plasmonics has led to significant advancement in real-time and ultrasensitive chemical and biological sensing and surface-enhanced spectroscopies, alkali metals featured by ideal free electron gas models have long been regarded as promising plasmonic materials but seldom been explored due to their high chemical reactivity. Here, we demonstrate the in operando plasmonic monitoring of the electrochemical evolution of lithium metal during battery cycling by taking advantage of selective electrochemical deposition. The relationships between the evolving morphologies of lithium metal and in operando optical spectra are established both numerically and experimentally: Ordered growth of lithium particles shows clear size-dependent reflective dips due to hybrid surface plasmon resonances, while the formation of undesirable disordered lithium dendrites exhibits a flat spectroscopic profile with pure suppression in reflection intensity. Under the in operando plasmonic monitoring enabled by the microscopic morphology of metal, the differences of lithium evolutionary behaviors with different electrolytes can be conveniently identified without destruction. At the intersection of energy storage and plasmonics, it is expected that the ability to actively control and in operando plasmonically monitor electrochemical evolution of lithium metal can provide a promising platform for investigating lithium metal behavior during electrochemical cycling under various working conditions.

lithium metal | battery | plasmonic | in operando | monitoring

The lithium metal battery, which features the highest specific capacity (3,860 mAh g^{-1}) and the lowest electrochemical potential (−3.04 V versus the standard hydrogen electrode) is regarded as the most promising candidate for next-generation energy storage devices (1). A fundamental understanding as well as real-time monitoring and control of the electrochemical evolution of reactive lithium metals are essential for the development of lithium metal-based energy storage devices (1). One of the most important issues is the formation of dendrites during repeated cycling of lithium plating and stripping processes, which not only severely decreases the coulombic efficiency and cycle life, but also triggers serious safety hazards in the absence of timely control (2). Although great efforts have been made to suppress dendrite formation, such as artificial solid-electrolyte interphase (3, 4), nanoscale interface engineering (5), stable hosts for guided lithium deposition (6, 7), and new liquid electrolytes and additives (8, 9), the dynamic behavior of lithium metal during electrochemical cycling under drastically different working conditions still remains largely elusive and cannot be precisely monitored and/or controlled. Therefore, there have been great efforts to develop in operando tools to provide real-time information about the dynamics of lithium metal in a real working environment. However, the progress is rather limited because of the high chemical reactivity and weak atomic bonding of lithium, which make it a weak scatterer for electrons and X-rays (10, 11). Therefore, an in operando, nondestructive, and label-free technique is urgently required to provide a holistic monitoring of the dynamic morphological evolution of lithium metal. Alternatively, plasmonics arising from collective oscillations of the free electron gas density has been widely used for nondestructive, real-time, and sensitive chemical and biological detection (12–15) after decades of development. Alkali metals such as lithium and sodium with free electron gas behavior have long been theoretically predicted as promising plasmonic materials (16, 17) but have seldom been explored, primarily due to their high chemical reactivity (18).

Here, we demonstrate the in operando plasmonic monitoring of the electrochemical evolution of lithium metal during battery cycling by nondestructive real-time optical spectroscopies. The correlation between the spectroscopic features and the evolutionary morphologies of lithium metal is established both numerically and experimentally: The ordered deposition and growth of lithium particles exhibits discrete particle size-dependent plasmonic resonances in reflective spectra, whereas the undesirable formation of disordered dendrites exhibits a broadband antireflection feature with only mere intensity modulation due to random structure-featured plasmonic light trapping. The significant difference in the optical spectroscopies makes our platform powerful for the real-time monitoring of the evolution of lithium metal morphology and the detection of emergent

Significance

In operando and nondestructive technology is urgently needed to monitor and further control lithium metal morphology evolution for reviving lithium metal batteries. Taking advantage of lithium plasmonics, we developed an in operando plasmonic monitoring platform to investigate lithium deposition behavior in different working conditions and varied electrolytes. This technology, with a well-established correlation between the evolving morphologies of lithium metal and in operando optical spectra, can serve as an effective platform for investigating lithium morphology during electrochemical operations, which can further speed up new electrolyte design and the development of alkali metal-based energy storage systems.

Author contributions: L.Z. and J.Z. designed research; Y.J., L.Z., J.Y., and J.L. performed research; W.C., H.Z., and S.Z. contributed new reagents/analytic tools; Y.J., L.Z., W.C., H.Z., S.Z., and J.Z. analyzed data; and Y.J., L.Z., and J.Z. wrote the paper.

The authors declare no conflict of interest.

This article is a PNAS Direct Submission.

[1]To whom correspondence may be addressed. Email: linzhou@nju.edu.cn or jiazhu@nju.edu.cn.

This article contains supporting information online at www.pnas.org/lookup/suppl/doi:10.1073/pnas.1808600115/-/DCSupplemental.

lithium dendrites under various working conditions of battery operations.

Fig. 1 shows the plasmonic monitoring platform of lithium metal evolution by electrochemical reactions. The platform contains a planar battery (19) integrated with a reflection-mode optical microscope and an electrochemical control system (Fig. 1*A*). This planar battery is composed of ordered silver electrodes decorated on a tungsten metal film substrate, the lithium source ($LiFePO_4$), and liquid electrolyte (see *Methods* for detailed fabrication processes). As schematically illustrated in Fig. 1*A*, the ordered silver electrodes (20) on tungsten film are finely designed for selective deposition of lithium metal (*SI Appendix*, section 1), leading to effective monitoring of lithium evolution with high optical contrast. Lithium ions can be extracted from the $LiFePO_4$ cathode by applying a certain electrical current; the ions then move toward the anode, selectively nucleate from the ordered silver electrodes to alloy with silver first, and are finally reduced to lithium metal. The reversible electrochemical reactions ensure repeatable lithium plating and stripping processes, which enable the morphological evolution of deposited lithium metal. Affected by various factors such as interfacial chemistry and local current distributions, etc., lithium metal deposition will primarily evolve into two different pathways during battery operations. One is the ideal (normal) pathway for long-time stabilized battery operation, in which lithium metal tends to selectively nucleate on silver seeds more regularly to form periodic lithium particles with gradual size increases over the deposition time. The other is the nonideal (abnormal) pathway in which the undesirable formation of lithium dendrites is commonly triggered by uncertain fluctuations of chemical and/or electrical conditions. Once dendrites form, the deposited lithium will evolve much faster and more wildly, as indicated by the morphology of random lithium dendritic structures (Fig. 1*B*, *Lower*).

We first established the relationship between the lithium metal morphology and the optical spectrum by numerical calculations (Fig. 1*C*). The normally deposited lithium is modeled as graphite-arranged periodic hemispheres, while the lithium dendrites are modeled as random nanorods with random aspect ratios and orientations (see *Methods* for detailed optical modeling). For the normal lithium morphology (Fig. 1*B*, *Upper*), there are at least two types of optical modes: the localized surface plasmon (LSP), related to the isolated lithium particles; and Wood's anomaly (WA), related to the periodic geometry (*SI Appendix*, section 2). The periodic silver seeds serve as the initial state of the deposition process. As depicted in Fig. 1*C*, the referenced reflectance spectrum of the silver pattern (black solid line) shows a high intensity with unnoticeable plasmonic modes from 400 to 1600 nm. The rather weak optical modes of the silver seeds are primarily due to the significant impact from the unique tungsten film substrate, beneficial for the spectroscopic identification of lithium structure. But the WA modes of silver pattern, theoretically determined by the formula $\lambda_{WA} = 2\pi n_d/G_{mn}$ (21, 22), can still be identified from the reflection spectrum of that without tungsten film (*SI Appendix*, Fig. S5*A*). Here, n_d is the refractive index of the dielectric medium [$n_d = 1.42$ is used for the electrolyte of 1.0 M $LiPF_6$ in 1:1 vol/vol ethylene carbonate/diethyl carbonate with 2 wt % vinylene carbonate (23)], $G_{mn} = (4\pi/3a)\sqrt{m^2+n^2+mn}$ is the reciprocal vector provided by the metal surface, and $a = 577$ nm is the nearest space between adjacent silver seeds. After a short time of electrochemical deposition, the ideal or nonideal states of the evolved metal will exhibit different optical responses originating from the different morphologies in Fig. 1*B*, as illustrated in Fig. 1*C*. Under the normal operating conditions, the deposited lithium particles grow gradually, and the LSP modes of lithium particles exhibit red-shift with the increment of lithium particle diameter (*SI Appendix*, Figs. S2–S4), which revive the rather weak optical modes of silver triangles and enable remarkable reflection dips (Fig. 1*C*, *Upper*) as LSP modes approaching to WA modes. As the diameter of lithium particles increases from 200 to 350 nm (with respect to the increase of deposition time), λ_{LSP} shows controllable evolution from ~800 to 1200 nm. Note that the pronounced asymmetric profiles at ~800 and 1200 nm can be ascribed to the hybridizations of the LSP and WA, with amplified LSP observed around $WA_{1,0}$ at ~1230 nm and $WA_{1,1}$ at ~710 nm. A more systematically calculated mode–morphology correlation has been conducted as well (*SI Appendix*, Figs. S7 and S8), the significant spectroscopic amplification of which makes it ideal for the effective in operando plasmon detection of normal-deposited lithium metal. In contrast, the optical evolution of the

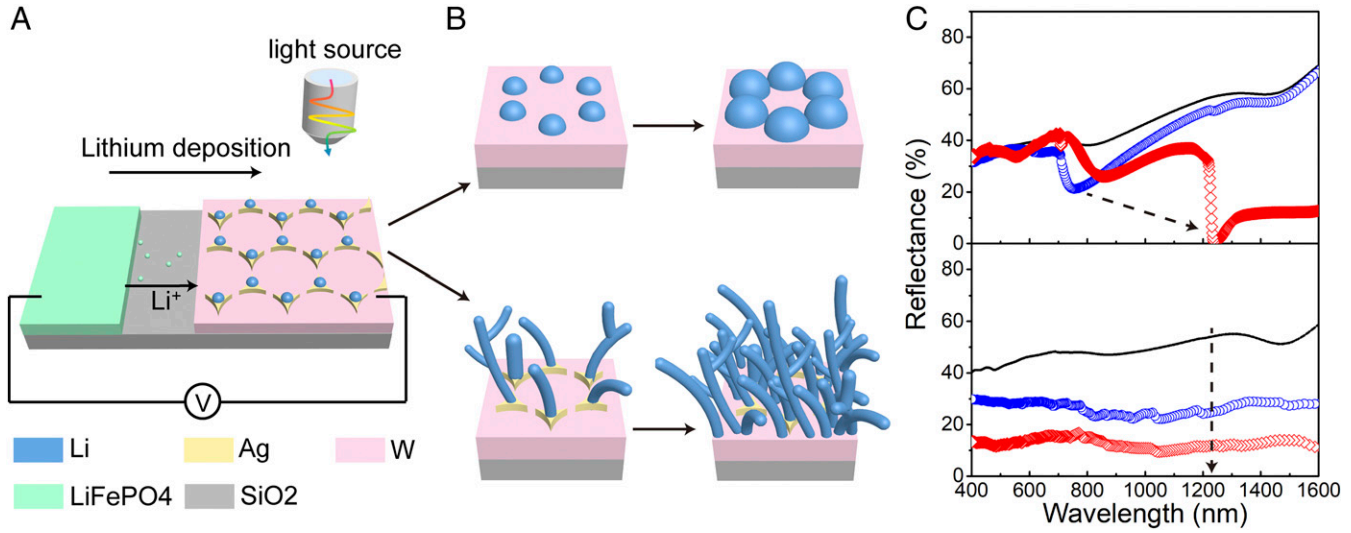

Fig. 1. In operando plasmonic monitoring of lithium morphological evolution in a battery. (*A*) Schematic of a planar battery device and in operando reflectance spectra measurement of the morphological evolution of lithium metal during electrochemical cycling. (*B*) Two pathways of lithium morphological evolution: growth of periodic lithium particle arrays (*Upper*) and formation of random lithium dendrites (*Lower*). (*C*) Simulated reflectance spectra of the two representative lithium morphological evolution pathways: growth of lithium hemisphere arrays (*Upper*) and formation of lithium dendrites (*Lower*). The arrows indicate the optical evolution tendency during lithium deposition.

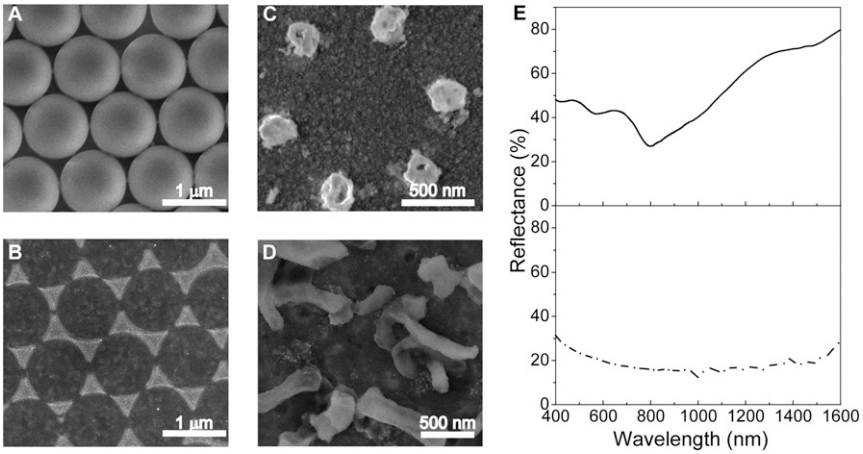

Fig. 2. SEM images at each step of fabrication and of two different lithium morphologies and ex situ reflectance measurements. (*A* and *B*) Detailed fabrication processes on the patterned electrodes for selective lithium deposition: SEM images of a closely packed monolayer of SiO_2 spheres with a diameter of 1 μm (*A*) and of silver triangles in a graphite-like arrangement (*B*). (*C* and *D*) Typical SEM images of the two representative lithium morphologies schematically illustrated in Fig. 1*B*: periodic array of lithium hemispheres (*C*) and random lithium dendrites (*D*). (*E*) Measured reflectance spectra of the two representative lithium morphologies in *C* and *D*: lithium hemispheres (*Upper*) and dendrites (*Lower*).

abnormal dendrite formation is quite different (Fig. 1*C*, *Lower*). The broadband antireflection (flat spectra) can be observed to have drastically attenuated reflectance (<10%), which stems from plasmonic light trapping by light scattering and coupling (24–27), as widely reported in the random particle-based broadband plasmonic absorbers (28, 29). This distinct difference of optical modes (instead of mere variation of intensity) between periodically controllable normal-lithium particles and random dendrites forms the basis of plasmonic monitoring of the morphological evolution of lithium metal during electrochemical cycling.

We then demonstrated the validity of the established correlation experimentally under ex situ conditions. The selective electrodes (20) (periodic silver triangles in Fig. 1*A*) were fabricated by angle-resolved nanosphere lithography (30, 31) in three steps: (*i*) closely packing a monolayer of SiO_2 spheres with a diameter of 1 μm (Fig. 2*A*), (*ii*) physically depositing silver, and (*iii*) removing the SiO_2 template by sonication. Fig. 2*B* depicts that the selective silver electrodes obtained have good periodicity. We then assembled the battery in Fig. 1*A* and operated it under different external fields. The electrochemical conditions for Fig. 2 *C* and *D* are 0.03 mA for 5 min and 1 mA for 2 min, respectively. Subsequently, two typical morphologies of lithium metal were observed (Fig. 2 *C* and *D*). Both the nanoparticles and dendrites produced in the experiment resemble the primary features modeled in Fig. 1*B*. The finite distortions of lithium particle shapes may result from the transient exposure to ambient atmosphere during the sample transfer process and electron beam irradiation in the scanning electron microscope chamber. Fig. 2*E* shows the measured spectra of the two samples, indicating good agreement with the respective calculated curves in Fig. 1*C*.

To further demonstrate the relationship between the optical spectra and lithium morphology, we measured the reflectance spectra during the lithium deposition process (Fig. 3). Two representative electrical currents (I = 0.03 and 1 mA) were applied to induce the two different evolution pathways: lithium particle growth and lithium dendrite formation, respectively. For the case I = 0.03 mA, the in operando reflection spectra were measured as shown in Fig. 3*A*. At the initial time of deposition (t = 0 s), the measured spectrum was flat from 400 to 1600 nm. During the process of electrochemical lithium deposition, the overall intensity of reflectance decreased gradually, and a clear dip at ∼800 nm was developed at t = 8 min. In addition, further deposition resulted in an additional dip at ∼1200 nm emerging at t = 18 min, which agrees with the tendency of the numerical model. The reflectance at λ = 1225 nm in Fig. 3*A* was extracted and is plotted versus time after normalization in Fig. 3*C*, which demonstrates the relatively slow and gentle evolution process during lithium particle growth. To further identify the ordered morphology of the lithium particles, we removed the current, disassembled the planar cell once the plasmonic modes (λp = 800 and 1200 nm) were identified, and examined the morphology under SEM, as illustrated in Fig. 3 *E* and *G*, respectively. It was confirmed that lithium tends to nucleate as discrete nanoparticles on silver triangles and that the average size was ∼190 and 370 nm, as suggested in Fig. 1*B*. More measured morphology-dependent reflection spectra are shown in *SI Appendix*, section 3. By subtracting both simulated and measured diameter-dependent optical modes (*SI Appendix*, Fig. S8), one can safely establish the quantitative morphology–spectrum relationship of normally deposited lithium, as depicted in the red line of Fig. 3*C*. Similar in operando optical measurements of lithium dendrite formation were performed with I = 1 mA. The measured reflectance spectrum remains flat in the range of 400 to 1600 nm. In addition, the reflectance decreased drastically to ∼10% at t = 5 s and remained stable (∼5%) after t = 45 s (Fig. 3*B*). To study the drastic transition, in operando spectra in a narrower wavelength range (1100 to 1300 nm) were measured (*SI Appendix*, Fig. S12). Compared with that of ordered particles, the evolution of normalized reflectance at λ = 1225 nm of lithium dendrites over time is plotted in Fig. 3*D*, which indicates the rapid dendrite growth process and is notably different from Fig. 3*C*. The SEM images of the evolved dendrites at t = 5 s and 85 s are presented in Fig. 3 *F* and *H*, respectively, resembling the main features predicted in Fig. 1. To further address the necessity of periodic silver pattern as electrodes, we performed the same in situ reflection measurements during lithium deposition with two substrates without periodic silver pattern (bare tungsten and random silver/tungsten substrate). Because of the random deposition site-dominated features, both cases possess almost flat spectra and similar intensity evolution profiles for both normal and abnormal lithium states, making them difficult for fast identification during in operando monitoring (*SI Appendix*, Fig. S11).

To further explore the plasmonic monitoring of the cycling performance, we also investigated the in operando optical

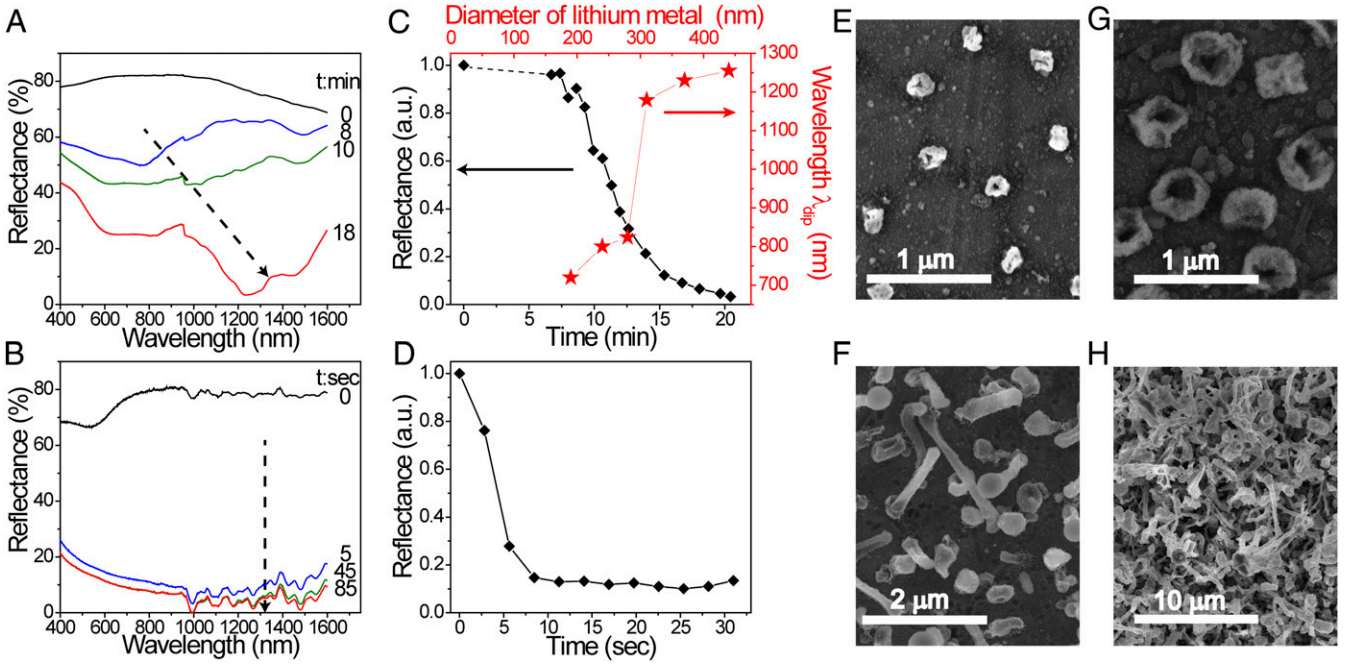

Fig. 3. In operando characterization of different pathways of lithium evolution. (*A* and *B*) In operando optical reflectance monitoring of the two representative lithium evolution pathways over time during electrochemical lithium deposition: growth of patterned lithium hemispheres (*A*) and formation of random dendrites (*B*). The dashed lines indicate the evolution tendency over time during lithium deposition. (*C* and *D*) Evolution of normalized reflectance at the wavelength of 1225 nm over the electrochemical deposition time of patterned lithium hemispheres (*C*) and random dendrites (*D*). The dashed line in *C* represents the voltage drop process until the deposition potential of lithium metal is reached. The red color in *C* represents the measured lithium particle diameter and corresponding dip in reflection spectra. (*E* and *G*) Typical SEM images of lithium morphologies indicating the two essential plasmonic modes, λp, observed at ∼800 nm (*E*) and ∼1200 nm (*G*). (*F* and *H*) SEM images of lithium dendrite morphology at the beginning and end of lithium deposition, respectively.

measurements of lithium deposition and stripping behaviors in a full electrochemical cycle of battery operation. Under the operating condition $I = 0.03$ mA, the reflection spectra of the structures during deposition (total deposition time of 15 min) and stripping are demonstrated in Fig. 4 *A* and *B*, respectively. It is evidenced that the typical plasmonic features of periodic lithium particles are well maintained in the in operando-measured spectra during both electrochemical cycling processes. The finite decrease in reflectance after the full cycle compared with the initial state can be ascribed to the solid-electrolyte interphase on the lithium metal surface (32). While under the operating condition $I = 1$ mA, the cycling of dendrites

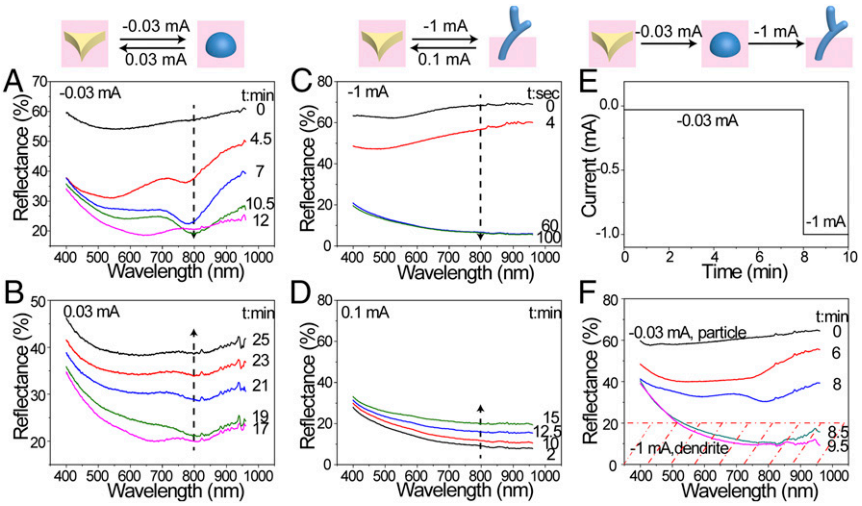

Fig. 4. In operando optical characterization of full electrochemical cycling and lithium dendrite detection. (*A*–*D*) In operando optical reflectance monitoring of the electrochemical evolution of patterned lithium hemispheres (*A* and *B*) and lithium dendrites (*C* and *D*) during lithium deposition (*A* and *C*) and stripping (*B* and *D*) with different applied electrical currents: $I = 0.03$ mA (*A* and *B*), $I = 1$ mA (*C*), and $I = 0.1$ mA (*D*). The total deposition time of lithium is 15 min for *A* and 2 min for *C*. (*E* and *F*) In operando lithium dendrite detection by real-time optical reflectance spectral monitoring: the applied current, *I*, as a function of time (*E*), and in operando reflectance spectra of the electrochemically tuned planar battery (*F*).

exhibits a very different spectroscopic feature. As shown in Fig. 4*C*, the measured reflectance decreased abruptly ($R < 10\%$) during lithium deposition (total deposition time of 2 min). Moreover, the reflectance was irreversible in the stripping process, even though operating at $I = 0.1$ mA (0.1 times the deposition current) for more lithium extraction (Fig. 4*D*), which is due to the side effects of lithium dendrites, such as the formation of dead lithium, lowering the coulombic efficiency (6).

Thus far, we have demonstrated that the pronounced discrepancy in the optical spectra between the ideal and nonideal morphologies can be used for in operando monitoring of lithium metal dynamics and for detecting the emerging formation of dendrites. To examine the detectability of dendrite formation during battery operations in a finite time span, we used a lower galvanostatic current ($I = 0.03$ mA) for the nucleation and growth of particles, followed by a higher current of $I = 1$ mA to accelerate the growth of the dendrites after $t = 8$ min (Fig. 4*E*). The spectroscopic features changed drastically in the real-time spectra at $t = 8$ min (Fig. 4*F*), indicating the formation of lithium dendrites between $t = 8$ min and $t = 8.5$ min, which confirmed the validity of the proposed plasmonic monitoring for real-time detection of dendrite formation in lithium metal batteries.

This in operando plasmonic monitoring platform can be used to monitor and effectively evaluate dynamic lithium deposition behaviors under various working conditions during real-time electrochemical operations. For example, electrolyte components, especially additives, have been heavily investigated to improve the electrochemical performance of lithium metal anodes (19, 33). However, most if not all of the previous studies have relied on ex situ characterizations, which cannot provide direct evidence and feedback. This in operando and nondestructive characterization method can provide a direct and real-time observation of whether the electrolyte can suppress dendrite formation, which is of vital importance for rapid electrolyte design and development. As an example of demonstration, three typical electrolytes commonly used in lithium metal batteries were selected for comparing the lithium metal behaviors under various applied electrical currents: (*i*) 1.0 M $LiPF_6$ in 1:1 vol/vol diethyl carbonate/ethylene carbonate with 2 wt % vinylene carbonate (designated $LiPF_6$); (*ii*) 1.0 M lithium bis (trifluoromethylsulfonyl)imide (LiTFSI) in 1:1 vol/vol 1,3-dioxolane (DOL)/1,2-dimethoxyethane (DME) (designated LiTFSI); and (*iii*) 1.0 M LiTFSI in 1:1 vol/vol DOL/DME with 1.0% $LiNO_3$ (designated LiTFSI + $LiNO_3$). As shown in Fig. 5*A*, in the battery using the electrolyte system of $LiPF_6$, the reflectance spectrum with a clear dip at ~800 nm was developed at a current of 0.1 mA, which indicates the ordered growth mode of lithium particles. As the applied current increased to 1 mA and 3 mA, the reflectance spectrums became flat with much suppressed reflectance, which is a clear indication of lithium dendrite formation (*SI Appendix*, Fig. S13). In the battery operated with LiTFSI, common for sulfur/lithium metal batteries (Fig. 5*B*), as the applied current increased from 0.1 mA to 3 mA, the in operando reflectance shows an evolution tendency similar to that of the $LiPF_6$ system. Lithium dendrite is formed at more than 1 mA, which is consistent with SEM images in *SI Appendix*, Fig. S14. For comparison, 1 wt % $LiNO_3$ was added to 1 M LiTFSI in DOL/DME (1:1 vol/vol) (Fig. 5*C*). $LiNO_3$ is frequently used as a shuttle-effect inhibitor and helps to improve the passivation and surface chemistry of the lithium metal surface (34–36). It is clear that the evolution of lithium metal in this system significantly differs from the two previous instances. The in operando reflectance shows a clear dip at 0.1, 1, and even 3 mA. SEM images at three applied current conditions confirm that lithium particles nucleate (*SI Appendix*, Fig. S15) with uniform and smooth morphologies and that dendrites are prevented, even at 3 mA. The distinct lithium evolution behaviors that the reflectance spectra revealed with different electrolyte systems demonstrate the accuracy, practicability, and multifunctionality of our in operando plasmonic monitoring platform.

In summary, we developed an in operando plasmonic monitoring technology that is able to quantitatively and rapidly analyze the morphology evolution of lithium metal under various operation and electrolyte conditions. Two different pathways of lithium metal morphology evolution can be identified by this developed nondestructive optical spectroscopy technology. It is expected that this technology can serve as a transformative platform for investigating lithium morphology during electrochemical operations. The technology of plasmonic monitoring may also help to speed up electrolyte design and development because of its facile and real-time advantages.

Methods

Fabrication of the Planar Lithium Metal Battery. The lithium source, deposited electrodes, and transparent electrolytes are the three essential components of a typical planar battery. To construct our planar battery, we employed $LiFePO_4$ as the lithium source, a tungsten film patterned with silver triangle arrays as the selective lithium deposition electrodes, and a liquid electrolyte (1.0 M $LiPF_6$ in 1:1 vol/vol ethylene carbonate/diethyl carbonate with 2 wt %

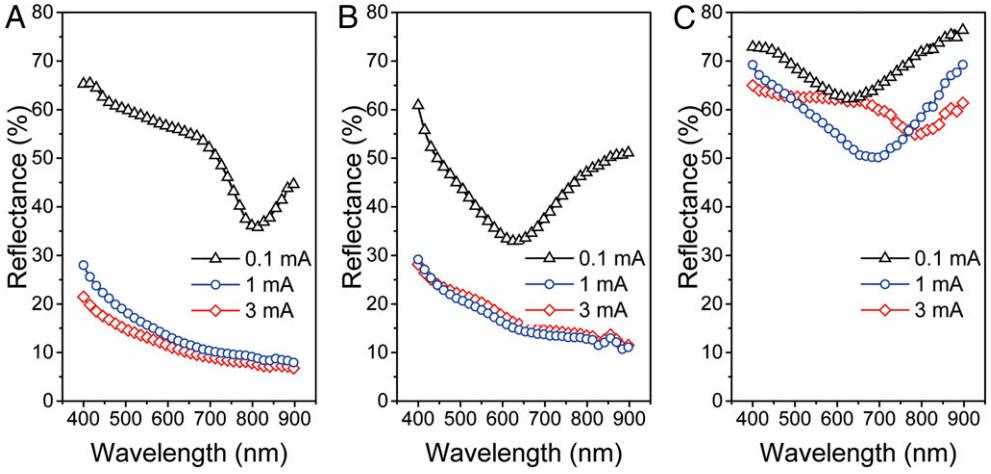

Fig. 5. In operando optical characterization and comparison of three different electrolyte systems. In operando optical reflectance of electrochemical lithium deposition behavior in electrolyte of 1.0 M $LiPF_6$ in 1:1 vol/vol diethyl carbonate/ethylene carbonate with 2 wt % vinylene carbonate (*A*), 1.0 M LiTFSI in 1:1 vol/vol DOL/DME (*B*), and 1.0 M LiTFSI in 1:1 vol/vol DOL/DME with 1.0% $LiNO_3$ (*C*) at varied currents.

vinylene carbonate; Zhangjiagang Guotai-Huarong New Chemical Materials Co.). The silver-patterned tungsten electrode was obtained in three steps: a tungsten film with a thickness of ~100 nm was deposited on a SiO_2 wafer (thickness ~1 mm) through physical vapor deposition (PVD) (Gatan 682 system). After that, a close-packed monolayer of SiO_2 spheres (diameter of 1 μm; Alfa Aesar) was spread on the top of the tungsten film by spin-coating SiO_2 solution [30% SiO_2 particles in ethanol/ethylene glycol (35 vol % each)] at a rotation speed of 5,000 rpm (37). The obtained SiO_2 monolayer was then used as the template for forming silver triangle arrays through PVD of a silver film (20 nm). The SiO_2 particles were removed by sonication. The silver pattern is on one side of the SiO_2 substrate, and a piece of $LiFePO_4$ conducted out by copper tape was put on the other side of the SiO_2 substrate. Two electrodes were entirely covered by another piece of SiO_2 substrate and sealed by epoxy resin with a hole left to fill with electrolyte. The device was then transferred into a glove box filled with argon gas, followed by the addition of electrolyte to fill the region between the silver triangle arrays and $LiFePO_4$. Lastly, the whole battery was sealed by epoxy resin.

In Operando Optical Measurement. A system based on a microspectrophotometer (microscope objectives with 10× magnifications, PV20/30 from CRAIC Technologies) was employed to acquire the reflection spectra at a fixed test position (nearest area to the $LiFePO_4$ electrode), with the tungsten film soaked in electrolyte as the reference. The variation of relative reflectance is due to the different electrolyte thickness. At the same time, an electrochemical workstation (Biologic SP-20) was used to control the lithium deposition/stripping through galvanostatic cycling and to measure the time-dependent potentials.

Morphology Characterization. The morphologies and structures during the fabrication processes and lithium deposition were characterized by SEM (Dual-Beam FIB 235; FEI Strata). During ex situ characterization of the lithium morphology, the battery was opened in the argon glove box after lithium deposition and optical reflectance measurement, after which the electrode was rinsed with fresh diethyl carbonate and dried. Electrodes were mounted onto SEM stages and sealed in argon-filled transfer vessels for immediate SEM observation.

Numerical Simulation. The calculated reflectance spectra were performed by the finite-difference time-domain method (Lumerical FDTD Solutions V8.6). A broadband plane wave excitation (400 to 1600 nm) and periodic boundary conditions were applied to the modeled structure. Field and power monitors were used to collect the reflected signals and the in-plane field distributions of the structure. Throughout the entire simulation, periodic lithium particles and random lithium dendrites were modeled for the two observed representative evolution morphologies. To simulate the periodic lithium particles, the lithium hemispheres, together with the underlying silver triangle particles arranged in a graphitelike structure (the nearest particle distance, or the lateral period, was 577 nm), were used according to the experimental process. The irregular silver triangle geometry was generated by a uniform silver film subtracted from a close-packed air nanorod array (1000 nm in diameter). The silver triangle array and the underlying tungsten film, which are located on the quartz substrate, are 20 and 100 nm thick, respectively. The diameter of the lithium hemisphere was time dependent and determined by the observed ex situ state. To simulate the random lithium dendrite structure, the overall layered geometry was the same, except that the periodic lithium hemispheres were replaced by random lithium nanorods (simulated building blocks for dendrites). To simulate the original situation of lithium dendrites, the bottom position of a lithium dendrite with a diameter of 0.2 ± 0.07 μm, a length of 1 ± 0.3 μm, and a random orientation was fixed on each top of a silver triangle (refer to the SEM morphology in Fig. 2*D*). To simulate the observed lithium dendrite morphology, up to 200 lithium nanorods with random positions, sizes, and orientations were added in a much larger simulation region (3×3.46 μm). All of the material parameters of lithium, silver, tungsten, and SiO_2 originate from the Palik data (38). The background refractive index of the simulated region is set at 1.42 with regard to the representative liquid electrolyte (23).

ACKNOWLEDGMENTS. We acknowledge the microfabrication center of the National Laboratory of Solid State Microstructures for technical support. This work is jointly supported by grants from the National Key Research and Development Program of China (2017YFA0205700), the State Key Program for Basic Research of China (2015CB659300), the National Natural Science Foundation of China (11874211, 11574143, 21805132, 11621091, and 61735008), the Natural Science Foundation of Jiangsu Province (BK20180341), QingLan Project of Jiangsu Province, and the Fundamental Research Funds for the Central Universities (021314380135 and 021314380128).

1. Lin D, Liu Y, Cui Y (2017) Reviving the lithium metal anode for high-energy batteries. *Nat Nanotechnol* 12:194–206.
2. Xu W, et al. (2014) Lithium metal anodes for rechargeable batteries. *Energy Environ Sci* 7:513–537.
3. Li NW, Yin YX, Yang CP, Guo YG (2016) An artificial solid electrolyte interphase layer for stable lithium metal anodes. *Adv Mater* 28:1853–1858.
4. Zheng G, et al. (2014) Interconnected hollow carbon nanospheres for stable lithium metal anodes. *Nat Nanotechnol* 9:618–623.
5. Yang CP, Yin YX, Zhang SF, Li NW, Guo YG (2015) Accommodating lithium into 3D current collectors with a submicron skeleton towards long-life lithium metal anodes. *Nat Commun* 6:8058.
6. Lin D, et al. (2016) Layered reduced graphene oxide with nanoscale interlayer gaps as a stable host for lithium metal anodes. *Nat Nanotechnol* 11:626–632.
7. Liu Y, et al. (2016) Lithium-coated polymeric matrix as a minimum volume-change and dendrite-free lithium metal anode. *Nat Commun* 7:10992.
8. Ding F, et al. (2013) Dendrite-free lithium deposition via self-healing electrostatic shield mechanism. *J Am Chem Soc* 135:4450–4456.
9. Zhang T, Liao KM, He P, Zhou HS (2016) A self-defense redox mediator for efficient lithium-O-2 batteries. *Energy Environ Sci* 9:1024–1030.
10. Markowitz M, Boryta D (1962) Lithium metal-gas reactions. *J Chem Eng Data* 7: 586–591.
11. Egerton RF, Li P, Malac M (2004) Radiation damage in the TEM and SEM. *Micron* 35: 399–409.
12. Stewart ME, et al. (2008) Nanostructured plasmonic sensors. *Chem Rev* 108:494–521.
13. Liu N, Hentschel M, Weiss T, Alivisatos AP, Giessen H (2011) Three-dimensional plasmon rulers. *Science* 332:1407–1410.
14. Ding SY, et al. (2016) Nanostructure-based plasmon-enhanced Raman spectroscopy for surface analysis of materials. *Nat Rev Mater* 1:16021.
15. Brongersma ML, Halas NJ, Nordlander P (2015) Plasmon-induced hot carrier science and technology. *Nat Nanotechnol* 10:25–34.
16. Naik GV, Shalaev VM, Boltasseva A (2013) Alternative plasmonic materials: Beyond gold and silver. *Adv Mater* 25:3264–3294.
17. Blaber MG, Arnold MD, Ford MJ (2009) Search for the ideal plasmonic nanoshell: The effects of surface scattering and alternatives to gold and silver. *J Phys Chem C* 113:3041–3045.
18. Boltasseva A, Atwater HA (2011) Materials science. Low-loss plasmonic metamaterials. *Science* 331:290–291.
19. Bao W, et al. (2014) Approaching the limits of transparency and conductivity in graphitic materials through lithium intercalation. *Nat Commun* 5:4224.
20. Yan K, et al. (2016) Selective deposition and stable encapsulation of lithium through heterogeneous seeded growth. *Nat Energy* 1:16010.
21. Auguié B, Barnes WL (2008) Collective resonances in gold nanoparticle arrays. *Phys Rev Lett* 101:143902.
22. Giudicatti S, et al. (2010) Plasmonic resonances in nanostructured gold/polymer surfaces by colloidal lithography. *Phys Status Solidi A* 207:935–942.
23. McArthur MA, Trussler S, Dahn JR (2012) In situ investigations of SEI layer growth on electrode materials for lithium-ion batteries using spectroscopic ellipsometry. *J Electrochem Soc* 159:A198–A207.
24. Li XH, Choy WCH, Lu HF, Sha WEI, Ho AHP (2013) Efficiency enhancement of organic solar cells by using shape-dependent broadband plasmonic absorption in metallic nanoparticles. *Adv Funct Mater* 23:2728–2735.
25. Zhou L, Yu X, Zhu J (2014) Metal-core/semiconductor-shell nanocones for broadband solar absorption enhancement. *Nano Lett* 14:1093–1098.
26. Lee YJ, Ruby DS, Peters DW, McKenzie BB, Hsu JWP (2008) ZnO nanostructures as efficient antireflection layers in solar cells. *Nano Lett* 8:1501–1505.
27. Zhu J, et al. (2009) Optical absorption enhancement in amorphous silicon nanowire and nanocone arrays. *Nano Lett* 9:279–282.
28. Yan M, Dai J, Qiu M (2014) Lithography-free broadband visible light absorber based on a mono-layer of gold nanoparticles. *J Opt* 16:025002.
29. Zhang N, et al. (2015) Ultrabroadband metasurface for efficient light trapping and localization: A universal surface-enhanced Raman spectroscopy substrate for "All" excitation wavelengths. *Adv Mater Interfaces* 2:1500142.
30. Haynes CL, Van Duyne RP (2001) Nanosphere lithography: A versatile nanofabrication tool for studies of size-dependent nanoparticle optics. *J Phys Chem B* 105:5599–5611.
31. Haes AJ, et al. (2005) Plasmonic materials for surface-enhanced sensing and spectroscopy. *MRS Bull* 30:368–375.
32. Parimalam BS, MacIntosh AD, Kadam R, Lucht BL (2017) Decomposition reactions of anode solid electrolyte interphase (SEI) components with LiPF6. *J Phys Chem C* 121: 22733–22738.
33. Qian J, et al. (2015) High rate and stable cycling of lithium metal anode. *Nat Commun* 6:6362.
34. Aurbach D, et al. (2009) On the surface chemical aspects of very high energy density, rechargeable Li-sulfur batteries. *J Electrochem Soc* 156:A694–A702.
35. Pei A, Zheng G, Shi F, Li Y, Cui Y (2017) Nanoscale nucleation and growth of electrodeposited lithium metal. *Nano Lett* 17:1132–1139.
36. Rosenman A, et al. (2015) The effect of interactions and reduction products of LiNO3, the anti-shuttle agent, in Li-S battery systems. *J Electrochem Soc* 162:A470–A473.
37. Mihi A, Ocana M, Miguez H (2006) Oriented colloidal-crystal thin films by spin-coating microspheres dispersed in volatile media. *Adv Mater* 18:2244–2249.
38. Palik ED (1985) *Handbook of Optical Constants of Solids* (Academic, New York).